Electrostatic Charging of Nonpolar Colloids by Reverse Micelles

G. Seth Roberts, Rodrigo Sanchez, Roger Kemp, Tiffany Wood, and Paul Bartlett*

School of Chemistry, University of Bristol, Bristol BS8 1TS, U.K.

Received December 14, 2007. Revised Manuscript Received March 18, 2008

Colloids dispersed in a nonpolar solvent become charged when reverse micelles are added. We study the charge of individual sterically stabilized poly(methyl methacrylate) spheres dispersed in micellar solutions of the surfactants sodium bis(2-ethyl 1-hexyl) sulfosuccinate [AOT], zirconyl 2-ethyl hexanoate [Zr(Oct)₂], and a copolymer of poly(12-hydroxystearic acid)−poly(methyl methacrylate) [PHSA-PMMA]. Although the sign of the particle charge is positive for Zr(Oct)₂, negative for AOT, and essentially neutral for PHSA-PMMA, the different micellar systems display a number of common features. In particular, we demonstrate that over a wide range of concentrations the particle potential is a constant, independent of the number of micelles added and independent of the colloid size. A simple thermodynamic model, in which the particle charge is generated by the competitive adsorption of both positive and negative micelles, is in good agreement with the experimental data.

I. Introduction

Interactions between surface active materials and nonpolar suspensions of colloidal particles play a key role in many technologically important processes. It has been recognized for at least 50 years[1] that adding surfactants to a nonpolar suspension frequently results in particle charging. This phenomenon is important in many practical situations, including the formulation of electrophoretic image displays,[2–4] electrorheological fluids,[5] air-borne drug delivery systems,[6] drop-on-demand inkjet printing,[7] liquid electrostatic developers,[8,9] and liquid detergents[10] together with the prevention of asphaltene deposits in crude oil processing,[11] colloidal stabilization in supercritical CO_2,[12] flow electrification in petroleum handling,[13,14] and the synthesis of new materials.[15,16] It is surprising therefore that, given its technological significance, the mechanism of charging in solvents of low permittivity is not well understood.[7]

A nonpolar solvent is distinguished from a polar solvent by a low relative dielectric constant, ε_r, of typically around 2−5. The thermodynamics of charging in a liquid is controlled by the Bjerrum length λ_B,

$$\lambda_B = \frac{e^2}{4\pi\varepsilon_0\varepsilon_r k_B T},\tag{1}$$

which is the characteristic separation between two ions at which their Coulombic interactions are exactly balanced by the thermal energy ($k_B T$). Here e is the elementary charge and ε_0 is the vacuum permittivity. In water, where $\varepsilon_r = 80$ at 22 °C, λ_B is only 0.7 nm while for a typical oil such as dodecane ($\varepsilon_r = 2$) the Bjerrum length is some 40 times larger at $\lambda_B = 28.3$ nm. The large Bjerrum length in a nonpolar environment has two important consequences for colloids. First, the concentration of molecular ions is extremely small because the solvation energy of an ion scales[17] as $\lambda_B/2a$ where a is the ionic radius. Because of the practical absence of charge carriers in an oil, screening of electrostatic interactions is negligible and charge interactions are extremely long-ranged. To demonstrate this, consider the dissociation of the symmetric monovalent electrolyte A^+A^-,

$$A^+A^- \rightleftharpoons A^+ + A^-.\tag{2}$$

Applying the law of mass action to this chemical equilibrium yields an expression for the total number of free ions per unit volume,

$$\rho_{ion} = \sqrt{\frac{3\rho}{\pi a^3} \exp\left(\frac{-\lambda_B}{2a}\right)}\tag{3}$$

Here ρ is the number density of the electrolyte and the degree of dissociation is assumed small. Taking the radius of a molecular ion as $a = 0.25$ nm, eq 3 yields an ionic concentration of $\sim 10^{-13}$ mol dm^{-3}, for a solute concentration of 10 mM. The corresponding Debye length $\kappa^{-1} = 1/\sqrt{4\pi\lambda_B\rho_{ion}}$ is ~ 100 μm. A second distinctive feature of electrostatics in oils is the small value for the double-layer capacitance. The diffuse ion atmosphere around a charged colloid acts as a molecular condenser of capacitance, $C^d = \varepsilon_0\varepsilon_r(1 + \kappa R)/R$, in the Debye−Hückel limit.[18] For the low ionic strengths characteristic of nonpolar systems, this expression reduces to $C^d = \varepsilon_0\varepsilon_r/R$ so that the capacitance is typically some 40 times smaller in an oil than for a comparable aqueous environment. The result is that only a minute charge on a colloid in a nonpolar environment is sufficient to generate an appreciable

* To whom correspondence should be addressed. E-mail: p.bartlett@bristol.ac.uk.

(1) van der Minne, J.; Hermanie, P. *J. Colloid Sci.* **1951**, 7, 600–615.
(2) Chen, Y.; Au, J.; Kazlas, P.; Ritenour, A.; Gates, H.; McCreary, M. *Nature* **2003**, 423, 136–136.
(3) Jo, G. R.; Hoshino, K.; Kitamura, T. *Chem. Mater.* **2002**, 14, 664–669.
(4) Comiskey, B.; Albert, J. D.; Yoshizawa, H.; Jacobson, J. *Nature* **1998**, 394, 253–255.
(5) Hao, T. *Adv. Mater.* **2001**, 13, 1847–1857.
(6) Jones, S. A.; Martin, G. P.; Brown, M. B. *J. Pharm. Sci.* **2006**, 95, 1060–1074.
(7) Morrison, I. D. *Colloids Surf.* **1993**, 71, 1–37.
(8) Croucher, M. D.; Lok, K. P.; Wong, R. W.; Drappel, S.; Duff, J. M.; Pundsack, A. L.; Hair, M. L. *J. Appl. Polym. Sci.* **1985**, 30, 593–607.
(9) Pearlstine, K.; Page, L.; Elsayed, L. *J. Imag. Sci.* **1991**, 35, 55–58.
(10) Van Der Hoeven, P. C.; Lyklema, J. *Adv. Colloid Interface Sci.* **1992**, 42, 205–277.
(11) Leon, O.; Rogel, E.; Torres, G.; Lucas, A. *Petroleum Sci. Technol.* **2000**, 18, 913–927.
(12) Ryoo, W.; Dickson, J. L.; Dhanuka, V. V.; Webber, S. E.; Bonnecaze, R. T.; Johnston, K. P. *Langmuir* **2005**, 21, 5914–5923.
(13) Touchard, G. *J. Electrostatics* **2001**, 51−52, 440–447.
(14) Tolpekin, V. A.; van den Ende, D.; Duits, M. H. G.; Mellema, J. *Langmuir* **2004**, 20, 8460–8467.
(15) Leunissen, M. E.; Christova, C. G.; Hynninen, A.-P.; Royall, C. P.; Campbell, A. I.; Imhof, A.; Dijkstra, M.; Roij, R.v.; Blaaderen, A. v. *Nature* **2005**, 437, 235–239.
(16) Bartlett, P.; Campbell, A. I. *Phys. Rev. Lett.* **2005**, 95, 128302.

(17) Parsegian, A. *Nature* **1969**, 221, 844–846.
(18) Lyklema, J. *Fundamentals of Interface and Colloid Science. Volume II: Solid-Liquid Interfaces*; Academic Press: London, 1995.

surface potential. For instance, Hsu et al. measured particle charges as low as 200−900 electrons on 800 nm nonaqueous colloids.[19] The corresponding surface potentials were −140 mV ($e\varphi/k_BT$ = −5.5) and comparable to typical values measured in highly charged aqueous colloids. These levels of potentials generate strong electrostatic repulsions. The contact value of the interaction potential (in units of k_BT) between two colloidal spheres of radius R and charge eZ_0 is, from Coulomb's law,

$$\frac{U_0}{k_BT} = \frac{1}{k_BT}\frac{Z_0^2e^2}{8\pi\varepsilon_0\varepsilon_rR} = \left(\frac{\lambda_B}{2R}\right)Z_0^2 \qquad (4)$$

A 1 μm particle carrying a charge of 100 electrons, equivalent to a surface charge density of 1 μC m^{-2} (about 10^3 times smaller than typical aqueous colloids), will generate an electrostatic repulsion in a nonpolar solvent of ≈100 k_BT at contact. Clearly, provided colloidal particles can be efficiently charged, electrostatic interactions in a nonpolar solvent will be both strong and long-ranged.

While the mechanism of charge formation in aqueous colloids is fairly well understood[18] the situation in nonpolar suspensions is still far from clear.[7,10,20,21] Experiments suggest that the particle charge is a complex function of the nature of the particle surface and frequently the presence of trace amounts of water. In many of the systems studied to date, surfactants have been added to facilitate particle charging. The surfactants, which typically form reverse micelles in nonpolar solvents, play an interesting dual role in these systems. First, the presence of micelles enhances the particle charge—probably by stabilizing countercharges in the cores of micelles. Second, micelles limit the range of the subsequent charge repulsions.[19] The vast majority of uncharged reverse micelles exist in a dynamic equilibrium with a very small fraction of positively and negatively charged micelles, generated by thermal fluctuations. This low concentration of charged micelles screens the electrostatic interactions on long length scales. Morrison, in an extensive review of the literature,[7] proposed three plausible mechanisms to account for colloid charging in nonpolar surfactant systems: (A) preferential adsorption of molecular ions, surfactant aggregates, or charged micelles onto the surface of a particle; (B) dissociation of surface groups with the subsequent transfer of molecular ions into the cores of reverse micelles; and (C) the adsorption of surfactant aggregates onto the particle surface, their complexation with surface groups followed by the exchange and desorption of the molecular ions into solution micelles. Much of the evidence for these mechanisms has come from electrokinetic and adsorption measurements, although recently surface force measurements[22,23] have provided direct evidence of long-range electrostatic repulsions in a nonpolar solvent.

The picture which has emerged to date is that the charging mechanism in nonpolar environments is more subtle than that encountered in aqueous systems. A signature of this complexity is the dependence of zeta potential on surfactant concentration.[24] Focusing on colloids dispersed in low-dielectric solvents using

AOT (Aerosol-OT, sodium bis(2-ethyl-1-hexyl)sulfosuccinate) several studies have reported that with increasing surfactant concentration the particle potential either monotonically decreases,[25] or more commonly display a maximum.[26,27] Keir et al.[27] report a highly monotonic dependence of the charge of silica in decane, which they explain qualitatively in terms of a competition between the surface binding of negative sulfosuccinate anions at low surfactant concentration and positively charged species at high [AOT] (mechanism A). Similar arguments have been invoked by McNamee et al.[23] to account for the maximum in the interaction forces measured between two hydrophobic silica surfaces at 100 mM AOT, and by Smith et al.[25] for the gradual reduction in the zeta potential of hydrophobic TiO$_2$ colloids seen with increasing [AOT]. In marked contrast to these observations, Hsu et al.[19] report the striking finding that the surface potential of sterically stabilized PMMA colloids, determined by both electrokinetic and direct interaction measurements, is *independent* of AOT concentration. They propose that the different dependence of the particle charge on [AOT] is a consequence of a change in the mechanism of charging—the polymer-coated PMMA particles charge by dissociation of surface groups (mechanism B) rather than by the adsorption of ionic species which is more frequently invoked in the case of AOT.

In this paper we re-examine the mechanism of charging of sterically stabilized colloids in low-permittivity solvents by using the recently developed[28] technique of single-particle optical microelectrophoresis (SPOM). An important advantage of this technique is its accuracy and sensitivity. Surface charges on the level of a few elementary charges can be reliably detected on individual colloidal particles with an uncertainty of about 0.25e. To gain a broad insight into the mechanism of charging in nonpolar solvents we focus on a simple model polymer-stabilized colloid with a well-defined surface chemistry and explore the particle charge produced by different species of reverse micelles. We study two surfactant and one polymeric system—AOT, Zr(Oct)$_2$ [zirconyl 2-ethyl hexanoate], and the copolymer PHSA−PMMA [poly(12-hydroxystearic acid)-g-poly(methyl methacrylate)]—each of which forms reverse micelles in dodecane. Although, our particles become negatively charged in the presence of AOT, positive on addition of Zr(Oct)$_2$, and remain essentially uncharged when PHSA−PMMA is added, we find several similarities in the electrokinetics of these chemically different systems which suggests that a common physical mechanism operates in each. By combining accurate electrokinetic measurements with adsorption measurements we propose that polymer-grafted particles charge by the simultaneous adsorption of *both* positively charged and negatively charged reverse micelles. A statistical model of the competitive adsorption of oppositely charged reverse micelles onto a spherical particle is analyzed and shown to be consistent with the experimental data.

II. Experimental Section

Colloidal Particles. Nonpolar sterically stabilized poly(methyl methacrylate) (PMMA) colloids were synthesized by a dispersion polymerization procedure, which has been described elsewhere.[29] The radius of the particles was varied by adjusting the initial monomer concentration. All particles studied contained no fluorescent dyes.

(19) Hsu, M. F.; Dufresne, E. R.; Weitz, D. A. *Langmuir* **2005**, *21*, 4881–4887.

(20) Parfitt, G. D.; Peacock, J. Stability of Colloidal Dispersions in Nonaqueous Media. In *Surface and Colloid Science: Volume 10.*; Matijevic, E., Ed.;Surface and Colloid Science; Plenum Press: New York, 1978; pp 163−226.

(21) Kitahara, A. Nonaqueous systems. In *Electrical Phenomena at Interfaces: Fundamentals, Measurements and Applications*; Ohshima, H., Furusawa, K., Eds., 2nd ed.; Marcel Dekker: New York, 1998; Chapter 4.

(22) Briscoe, W. H.; Horn, R. G. *Langmuir* **2002**, *18*, 3945–3956.

(23) McNamee, C. E.; Tsujii, Y.; Matsumoto, M. *Langmuir* **2004**, *20*, 1791–1798.

(24) Kitahara, A.; Amano, M.; Kawasaki, S.; Kon-no, K. *Colloid Polym. Sci.* **1977**, *255*, 1118–1121.

(25) Smith, P. G.; Patel, M. N.; Kim, J.; Milner, T. E.; Johnston, K. P. *J. Phys. Chem. C* **2007**, *111*, 840–848.

(26) Kitahara, A.; Satoh, T.; Kawasaki, S.; Kon-No, K. *J. Colloid Interface Sci.* **1982**, *86*, 105–110.

(27) Keir, R. I.; Suparno; Thomas, J. C. *Langmuir* **2002**, *18*, 1463–1465.

(28) Roberts, G. S.; Wood, T. A.; Frith, W. J.; Bartlett, P. *J. Chem. Phys.* **2007**, *126*, 194503.

(29) Antl, L.; Goodwin, J. W.; Hill, R. D.; Ottewill, R. H.; Owens, S. M.; Papworth, S.; Waters, J. A. *Colloids Surf.* **1986**, *17*, 67–78.

Table 1. Mean Radius R and Radius Polydispersity σ_R of the Colloidal PMMA Particles Used

	stabilizer	R (nm)	σ_R
RK1	A	42	0.07 [a]
AD1	A	610	0.046 [b]
RS1	B	425	0.10 [c]
RS2	B	840	0.09 [c]
RS3	B	1830	0.09 [c]

[a] From X-ray scattering measurements. [b] Static light scattering. [c] Electron microscopy.

Table 2. Structural Properties of Reverse Micelles Used

	AOT	Zr(Oct)$_2$	PHSA-PMMA
geometry of reverse micelles	sphere	sphere	cylinder [a]
hydrodynamic radius r_h/nm	1.6	1.16	9.17 [b]
micelle volume v_m/nm^3	17.2	6.5	2380
association number	30	33	9
data source	Kotlarchyk et al.[31]	Keir et al.[32]	Papworth[33]

[a] Small-angle neutron scattering measurements[33] indicate that the polymeric micelles are 28 nm in length and have a radius of 5.2 nm. [b] The radius of the sphere with the same translational friction coefficient as the cylindrical micelles.

Electron microscopy revealed that the particles were spherical and highly uniform in size with a mean radius R and a radius polydispersity σ_R (root-mean-square variation/mean radius) of less than 0.10. The results are summarized in Table 1. The particles were stabilized against aggregation by an ~10 nm thick grafted polymer layer. The stabilizer was composed of a polymeric comb of 50 wt % poly(12-hydroxystearic acid) (PHSA) 'teeth' and a backbone consisting of 45 wt % PMMA and 5 wt % poly(glycidyl methacrylate) (PGMA). The polymeric stabilizer was covalently attached to the particle surface. The PHSA teeth are soluble in aliphatic hydrocarbons, while the PMMA−PGMA backbone is insoluble so that the layer thickness is determined by the extended length of the PHSA chains. Two batches of stabilizer were used, with slightly different molecular weight distributions, as detailed in Table 1.

Micellar Solutions. We studied three different systems of reverse micelles in decane and dodecane. Small-angle neutron and X-ray scattering measurements reveal that each species forms well-defined reverse micelles at low concentrations. Literature data on the geometry and size of the reverse micelles are summarized in Table 2. AOT (Fluka BioChemika Ultra 99%) was purified by dissolution in methanol and tumbled with activated charcoal. The methanol was removed by rotary evaporation. The purity of the AOT was checked by a measurement of the limiting air−water surface tension. The value obtained of 27.1 ± 0.1 mN m^{-1} is in excellent agreement with previously reported values.[30] Any increase in the water content was minimized by storing the purified surfactant in a desiccator at all times prior to use. Zirconyl 2-ethyl hexanoate (Zr(Oct)$_2$) was purchased from Alfa Aesar (Heysham, UK) and came as a solution in mineral spirits. The solvent was evaporated off under vacuum at 80 °C, and the surfactant was redispersed in dodecane. The polymeric PHSA−PMMA copolymer (batch A) was identical to the grafted stabilizer on the 42 and 610 nm PMMA colloidal particles. Analysis by GPC gave a number-average molecular weight of M_n = 12 550 and a weight-average molecular weight of M_w = 83 400. The PHSA−PMMA copolymer was purified by precipitation from cold methanol, dried at 45 °C overnight and redissolved in dodecane at 140 °C. Micellar solutions were prepared in either dodecane (Acros, 99%) or decane (Acros, 99%), which were dried with activated molecular sieves (Acros, size 4A) prior to use.

Dispersion Formulation. The particle dispersions were prepared by mixing surfactant stock solutions with surfactant-free particle dispersions in dried dodecane or decane. Samples were shaken vigorously before being left for 24 h to equilibrate prior to any measurements. All solutions were sealed and stored under dry nitrogen to minimize water adsorption. The volume fraction of surfactant ϕ_m was calculated by assuming ideal mixing behavior and using the densities[32–34] of decane (0.73 g cm^{-3}), dodecane (0.75 g cm^{-3}), AOT (1.13 g cm^{-3}), Zr(Oct)$_2$ (2.15 g cm^{-3}), and PHSA−PMMA (1.04 g cm^{-3}).

Conductivity Measurements. Conductivities of the micellar solutions and dispersions were measured using a cylindrical concentric stainless steel conductivity probe (Model 627, Scientifica) at 22 °C. Measurements were made at an operating frequency of 15 Hz. The micellar solutions had conductivities in the range $10^{-1} \lesssim \sigma/\text{pS cm}^{-1} \lesssim 10^3$. The conductivity of the dried decane and dodecane used as solvents was recorded as <0.03 pS cm^{-1}. The excess ion concentration in the particle dispersions was estimated by centrifuging samples at 12 000 rpm for 2 h and measuring the conductivity of the upper particle-free supernatant. The viscosity of the micellar solutions was measured with a capillary Cannon Fenske viscometer operating at 25 °C. The viscosity of dodecane at this temperature is η = 1.383 mPa s.

Single-Particle Optical Microelectrophoresis (SPOM). The electrophoretic mobility of individual colloidal particles was measured from the change in the thermal fluctuations of a particle held in an optical tweezer trap and driven by an applied sinusoidal electric field. The theory underlying the technique of SPOM is discussed in detail elsewhere.[28] To perform a measurement a micropipette was used to transfer ~100 μL of a dilute suspension of particles (colloid volume fraction ~3 × 10^{-5}) into an electrophoresis cell. The purpose-built cell consisted of two parallel platinum electrodes mounted in a cylindrical glass chamber and sealed with a microscope coverslip. The electrode separation was measured as 189 μm. An individual colloidal particle was optically trapped in three dimensions using the radiation pressure from a tightly focused laser beam (λ = 1064 nm). A sinusoidal voltage with an amplitude of 5 V and a frequency of 17.5 Hz was applied. The modulation of the Brownian motion of the trapped particle produced by the applied field was measured with nanometer accuracy using an interferometric position detector. The position of the Brownian particle was collected every 10 μs for a total duration of 26 s. For each sample, data from at least 50 different individual particles was acquired, each of duration 26 s. The position detector readings were converted into particle displacements $\Delta x(\tau)$ in the time interval τ by recording the time-dependent mean-square voltage $\langle \Delta V^2(\tau) \rangle$ of five particles from the same batch of particles, with no applied field. Since the signal recorded is proportional to the displacement, $\langle \Delta V^2(\tau) \rangle$ was fitted to the theoretical expression for the mean-squared displacement $\langle \Delta x^2(\tau) \rangle$ of a Brownian sphere in a harmonic potential to yield the detector calibration and the corner frequency ω_c of the optical trap.

We extract the electrophoretic mobility of an individual particle by calculating the spectral density $I(\Omega)$ of its Brownian fluctuations using a discrete Fourier transform. The spectrum is a sum of a Lorentzian, characteristic of Brownian motion in a harmonic potential, together with a sharp peak at the applied electric field frequency ω_p. Integrating the spike in the power spectrum over the frequency axis yields the mean-square periodic displacement P_{sig} of the particle. The electrophoretic mobility μ of each particle sampled was calculated from the expression.[28] $\mu^2 E^2 = 2P_{sig}(\omega_p^2 + \omega_c^2)$ where E is the applied electric field. The sign of μ was determined by reducing the field frequency and following the oscillatory motion of the particle directly.

The electrophoretic mobilities of between 50 and 100 randomly chosen particles were determined from each sample. The mean mobility $\bar{\mu}$ and the charge polydispersity $\sigma_Z = \sqrt{\langle (Z - \bar{Z})^2 \rangle}/|\bar{Z}|$ were evaluated. For details of the procedure used to determine σ_Z, the reader is referred to the original report.[28] Variation of $\bar{\mu}$ with applied field was measured using electric fields of up to $E = 8 \times 10^4$ V m^{-1}. No dependence of $\bar{\mu}$ on E was observed. O'Brien and White[35] solved

(30) Nave, S.; Eastoe, J.; Penfold, J. *Langmuir* **2000**, *16*, 8733–8740.

(31) Kotlarchyk, M.; Huang, J. S.; Chen, S. H. *J. Phys. Chem.* **1985**, *89*, 4382–4386.

(32) Keir, R. I.; Watson, J. N. *Langmuir* **2000**, *16*, 7182.

(33) Papworth, S. *Ph.D. thesis, University of Bristol*, 1993.

(34) Bergenholtz, J.; Romagnoli, A. A.; Wagner, N. J. *Langmuir* **1995**, *11*, 1559–1570.

linearized versions of the coupled Navier−Stokes and Poisson−Boltzmann equations, arguing that in most cases of interest the charge cloud around each particle is only slightly distorted by the external field so that the particle mobility μ will be independent of E. Their linear analysis is valid provided that the applied field E is small compared with the electric field generated within the double layer, i.e., the condition $|E| \ll \kappa|\varphi|$ holds, where φ is the surface potential. When $|E| \gg \kappa|\varphi|$ the particle mobility is expected to become field-dependent. In the majority of the measurements reported here the field applied was less than $\kappa\varphi$ and the O'Brien and White analysis is valid. However, for a small number of samples, those with high charges and long screening lengths, the applied field was comparable to $\kappa\varphi$. However, experiments revealed no variation of the mobility with E so deviations from the linear regime analyzed by O'Brien and White are either small or at least not detectable in our measurements. The standard electrokinetic model of of O'Brien and White was therefore used to convert all measured mobilities into equivalent zeta potentials.

III. Results

a. Concentration of Charged Micelles from Conductivity. Because of the low dielectric constant, reverse micelles in a solvent such as dodecane behave quite differently from charged micelles in an aqueous environment. While the total micellar charge must vanish because of electroneutrality the *net* charge on each micelle fluctuates, as mobile ions are exchanged between the hydrophilic cores when micelles collide with each other. Micelle ionization is driven by spontaneous thermal fluctuations with micelle migration in an electric field providing the main mechanism for electrical conduction in dilute micellar solutions in oil.[36–40]

The electrostatic energy of a micelle of radius r carrying an excess charge ze is $\beta U_{el}(z) = z^2\lambda_B/2r$, where $\beta = 1/k_BT$. If charges freely exchange between micelles then the net charge carried by each micelle will fluctuate in time. In thermal equilibrium, the probability $p(z)$ of an excess charge of ze is proportional to the Boltzmann weight, $p(z) \approx \exp(-\beta U_{el}(z))$. Since $U_{el}(z)$ increases quadratically with z, the number of multiply charged micelles is significantly smaller than the number of singly charged micelles. When the micelle size is much smaller than λ_B, the concentration of multiply charged micelles is practically negligible and may be ignored. The proportion of singly charged micelles is fixed by the position of equilibrium in the charge exchange reaction,

$$2 \text{ uncharged micelles} \overset{K}{\rightleftharpoons} \text{positive micelle} + \text{negative micelle} \quad (5)$$
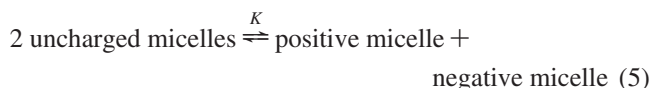
From the law of mass action, the equilibrium constant is $K = (n_+n_-)/n_0^2$ where n_+ and n_- are the number densities of charged micelles and n_0 is that of uncharged micelles. Because of the practical absence of free ions, $n_+ = n_-$. The fraction of ionized micelles, $\chi = (n_+ + n_-)/n_0$, is therefore $\chi = 2\sqrt{K}$. Rewriting the constant K in terms of the electrostatic energy of a singly charged micelle $\beta u_{el} = \lambda_B/2r$ gives the relation,

$$\chi = 2 \exp[-\beta u_{el}] \quad (6)$$

To elucidate the nature of the charging mechanism, we used three different reverse micellar systems. Conductivity measurements were used to characterize the degree of charge fluctuations

Table 3. Viscosity and Conductivity of Micellar Solutions in Dodecane

	AOT	Zr(Oct)$_2$	PHSA−PMMA
intrinsic viscosity, $[\eta]$	2.5	3.4	7.4
fraction of ionized micelles, χ	1.5×10^{-5}	2.7×10^{-5}	3.2×10^{-2}
electrostatic charging energy, βu_{el}	11.8	11.2	4.2

in each of the solutions. For monovalent, same-sized micelles the conductivity σ is

$$\sigma = \frac{e^2(n_+ + n_-)}{\xi} \quad (7)$$

where ξ is the micellar friction coefficient, which depends upon the size and shape of the micelle. To discuss both spherical and cylindrical micelles, we write $\xi = 6\pi\eta r_h$, where r_h is the equivalent spherical hydrodynamic radius of the micelle. In the case of a spherical micelle $r_h = r$, while for a cylindrical micelle of length l and diameter d, the equivalent radius is[41,42]

$$r_h = \frac{l/2}{\ln p + \gamma} \quad (8)$$

where $p = l/d$ is the axial ratio and γ is an end-effect correction. Tirado and de la Torre,[42] have shown that in the range $2 \leq p \leq 20$ relevant here, the hydrodynamics of rods are reproduced by the quadratic expression, $\gamma = 0.312 + 0.565/p − 0.1/p^2$. Replacing the micelle number density by the volume fraction $\phi_m = n_0 v_m$, where v_m is the micelle volume, it follows immediately from eq 7 that if micelle charging by spontaneous fluctuations is the dominant mechanism the conductivity of a dilute micellar solution should obey the simple expression,

$$\sigma = \frac{e^2}{6\pi r_h \eta v_m}\chi\phi_m \quad (9)$$

The application of this equation is complicated by the fact that the solution viscosity η is also a function of the micelle concentration ϕ_m. In the dilute regime, the relative viscosity (normalized by the solvent viscosity η_0) may be written in terms of the virial expansion, $\eta/\eta_0 = 1 + [\eta]\phi_m + ...$ where quadratic and higher terms have been neglected and $[\eta]$ is the Einstein coefficient. To allow for the concentration dependence of the viscosity, capillary viscometry was used to follow the viscosity of each micellar solution. The values obtained for $[\eta]$ are listed in Table 3. For hard spheres, the Einstein coefficient is 2.5. Comparison with the value measured for AOT suggests that the hard sphere diameter of the AOT micelles is accurately given by Table 2. The slightly higher Einstein coefficient observed in Zr(Oct)$_2$ is probably a consequence of the greater solvation of the surfactant tail layer and entrainment of solvent molecules which increases the molecular weight of the micelles and so increases $[\eta]$. The significantly larger Einstein coefficient measured for the PHSA−PMMA micelles may be accounted for at least qualitatively by the increased asymmetry of the micelles.

The charge fluctuation mechanism outlined above (eq 9) predicts that the product $\sigma\eta$ should depend linearly on the micelle volume fraction ϕ_m with a gradient, $\sigma\eta/\phi_m$, which for fixed micelle size and shape, is purely a function of the charge fraction χ. The conductivity σ and viscosity η of micellar solutions of AOT, Zr(Oct)$_2$, and the amphiphilic polymer PHSA−PMMA were measured (with no particles) as a function of volume fraction at

(35) O'Brien, R. W.; White, L. R. *J. Chem. Soc., Faraday Trans. II* **1978**, *74*, 1607.
(36) Eicke, H. F.; Borkovec, M.; Das-Gupta, B. *J. Phys. Chem.* **1989**, *93*, 314–317.
(37) Hall, D. G. *J. Phys. Chem.* **1990**, *94*, 429–430.
(38) Kallay, N.; Chittofrati, A. *J. Phys. Chem.* **1990**, *94*, 4755–4756.
(39) Kallay, N.; Tomic, M.; Chittofrati, A. *Colloid Polym. Sci.* **1992**, *270*, 194–196.
(40) Bordi, F.; Cametti, C. *Colloid Polym. Sci.* **1998**, *276*, 1044–1049.

(41) Hansen, S. *J. Chem. Phys.* **2004**, *121*, 9111–9115.
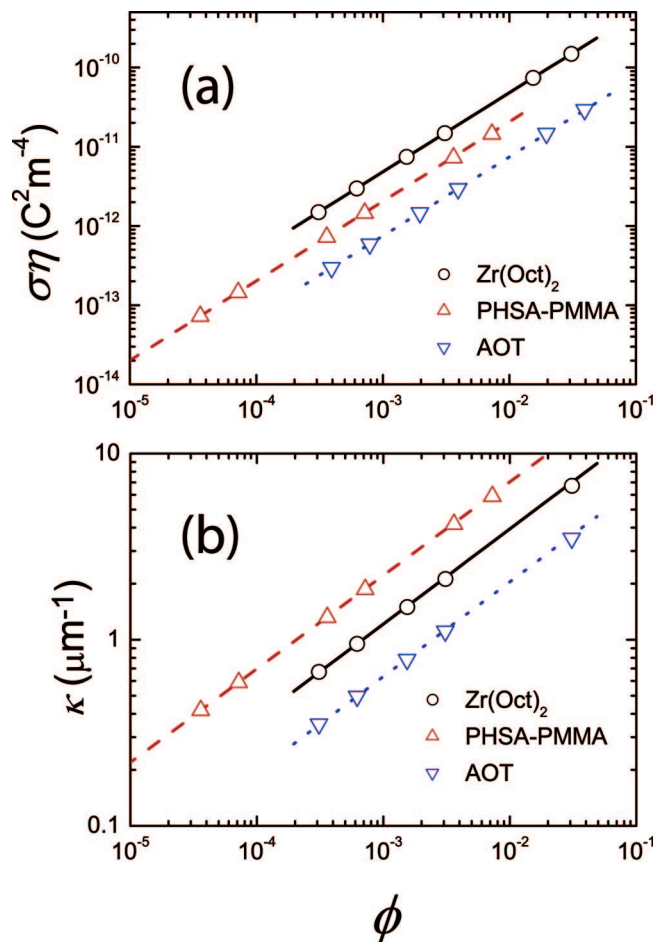(42) Tirado, M. M.; Torre, J. G. *J. Chem. Phys.* **1979**, *71*, 2581–2587.

Figure 1. (a) $\sigma\eta$ for reverse micellar solutions in dodecane (without particles) as a function of micelle volume fraction. The lines are of unit gradient. The symbols denote measurements and the lines denote fits to eq 9. (b) Inverse Debye lengths determined from conductivity data.

22 °C. Figure 1a shows the experimentally determined value of $\sigma\eta$ as a function of ϕ_m. In each case as the concentration of micelles was increased the conductivity increased, with a linear dependence of $\sigma\eta$ upon ϕ_m being seen over 2 orders of magnitude change in ϕ_m. From these measurements we used literature values for the size and shape of the reverse micelles formed (summarized in Table 2) and eq 9 to calculate the fraction χ of charged micelles. The derived values are summarized in Table 3 together with the corresponding estimates of the micelle charging energy u_{el}. The value obtained for AOT, the only system where data has previously been reported, is in excellent agreement with the results of an earlier study.[19] From the measured micelle charge fraction χ, we calculate the inverse Debye length $\kappa = \sqrt{4\pi\lambda_B(n_+ + n_-)}$. The resulting values are plotted in Figure 1b as a function of ϕ_m. Note that the electrostatic interactions between charged colloids suspended in these micellar solutions are long-ranged, with Debye lengths in the range of 0.1–10 μm.

b. Surface Potentials from Electrophoretic Mobilities. In the absence of micelles, our particles have a very small electrophoretic mobility and are essentially uncharged. The particles remain colloidally stable because of the dense grafted polymeric PHSA layer present. Sensitive SPOM measurements on individual PMMA spheres with a radius of 610 nm gave an electrophoretic mobility of $\bar{\mu} = -(2.9 \pm 0.2) \times 10^{-11}$ m^2 s^{-1} V^{-1} and a negative zeta potential φ of -3.6 ± 0.4 mV.[28] However, adding either 1 mM of AOT or 1.7 mM of Zr(Oct)$_2$ produced a dramatic change. Particles in the presence of Zr(Oct)$_2$ reverse
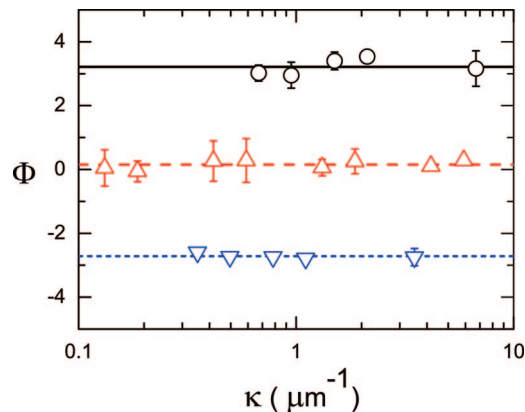

Figure 2. The scaled surface potential $\Phi = e\bar{\phi}/k_BT$ as a function of the inverse Debye length for PMMA particles of radius $R = 610 \pm 30$ nm. The figure shows data for PMMA particles with added Zr(Oct)$_2$ (circles), PHSA-PMMA (triangles), and AOT (inverted triangles). Note that for each micellar system Φ is independent of the inverse Debye length κ or equivalently the micelle concentration.

micelles developed a large positive charge ($\varphi = 82 \pm 5$ mV), and a large negative charge in the case of added AOT micelles ($\varphi = -70 \pm 2$ mV). The electrophoretic mobilities of identically sized particles treated with either AOT or Zr(Oct)$_2$ had very similar magnitudes ($\bar{\mu}_{AOT} = -(5.7 \pm 0.1) \times 10^{-10}$ m^2 s^{-1} V^{-1} and $\bar{\mu}_{Zr} = (6.4 \pm 0.3) \times 10^{-10}$ m^2 s^{-1} V^{-1}) but opposite signs. As the concentration of AOT was increased from 1 to 100 mM and Zr(Oct)$_2$ from 1.7 to 170 mM the electrophoretic mobilities and zeta potentials of both systems remained essentially unaltered. Addition of PHSA−PMMA solutions to our particles, at comparable levels to the AOT and Zr(Oct)$_2$ surfactants, gave no identifiable change in mobility ($\bar{\mu} = 3.5 \times 10^{-11}$ m^2 s^{-1} V^{-1}, $\varphi = 4 \pm 3$ mV). The particles remained essentially uncharged.

Adding reverse micelles to a nonpolar suspension has two consequences. First, it leads to particle charging and second, as discussed in Section III.a, it produces an increase in the concentration of charged micelles in solution and thus a reduction in the Debye length κ^{-1}. Using the data presented in Figure 1b, we estimate the dimensionless inverse Debye length κR for each micelle concentration. Figure 2 shows the scaled particle potential $\Phi = e\bar{\phi}/k_BT$ calculated from the mean mobility $\bar{\mu}$, using the method of O'Brien and White.[35] While the values for Φ are different in each of the three systems studied, the variation of Φ with κ is strikingly similar. In each case, we find that the surface potential is independent of the number of micelles added, over a change of 10^2 in concentration. We find $\Phi = -2.72 \pm 0.07$ for AOT ($0.21 \leq R \leq 2.1$), $\Phi = 3.2 \pm 0.2$ for Zr(Oct)$_2$ ($0.41 \leq R \leq 4.1$), and $\Phi = 0.15 \pm 0.13$ for PHSA−PMMA ($0.08 \leq R \leq 3.6$).

Despite the micelles of AOT, Zr(Oct)$_2$ and PHSA-PMMA being chemically different we see several qualitative similarities. A key finding is that the surface potential is essentially independent of the number of micelles added. This observation agrees with the results of more limited experiments on the AOT/PMMA system reported by Hsu et al..[19] In Section IV we show that our observations are compatible with the assumption of an amphoteric charging mechanism in which the particle charge is generated by the adsorption simultaneously of *both* positive and negatively charged species. Dissociation or absorption of a single species, either positive or negative depending on the surfactant system used, is inconsistent with the experimental observation of a constant surface potential Φ. For instance, if the particle charge was produced by ionization of a specific surface group with the counterions being solubilized in the continuous phase then
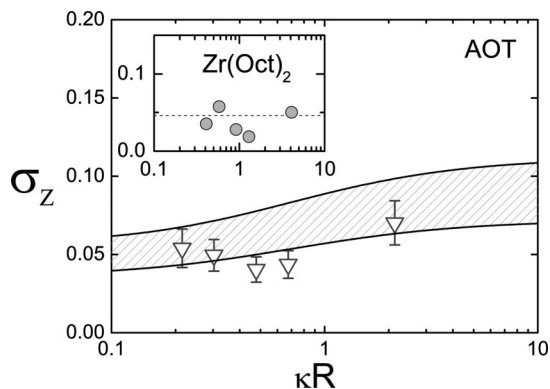
Figure 3. Variation of the charge polydispersity σ_Z with κR. Conditions: PMMA particles of radius $R = 610$ nm with added AOT (inverted triangles, main figure) or Zr(Oct)$_2$ (circles, inset). The hashed region indicates the charge polydispersity calculated assuming a constant surface potential ($\Phi = 2.72$) and a size polydispersity of between 0.056 (top boundary) and 0.036 (bottom boundary). The region indicates the uncertainty in the expected values of $\langle\sigma_Z\rangle$ given the measured radius polydispersity $\langle\sigma_R\rangle = 0.046 \pm 0.01$.

increasing micelle concentration would result in an increase in the charge as more micelles became available in which the counterion could be accommodated. Conversely, if the mechanism was adsorption of a single species then adding more micelles would lead to greater adsorption and an increased particle charge.

The raw data of the SPOM measurements is a scatter plot of effective charge with one point from each individual particle. From these data, a charge distribution $P(Z)$ was determined. In all cases this distribution was well fitted by a Gaussian of width σ_Z defined by

$$\sigma_Z = \frac{1}{|\bar{Z}|}\Big(\int_0^\infty P(Z)(Z - \bar{Z})^2\Big)^{1/2}. \qquad (10)$$

Figure 3 displays the variation of $\langle\sigma_Z\rangle$ with κR following the addition of AOT to a suspension of 610 nm PMMA particles. The charge distribution is surprisingly narrow with a width that is of order the size polydispersity of the particles used, $\langle\sigma_R\rangle = 0.046 \pm 0.01$. Although the quality of data for the case of the Zr(Oct)$_2$ surfactant (inset of Figure 3) is poor, it is evident that in this system also the values for the charge and size polydispersities are comparable. The numerical correspondence between $\langle\sigma_Z\rangle$ and $\langle\sigma_R\rangle$ may be explained by assuming that the surface potential is not only constant at different screening length but also for different sized particles. In the nonlinear Poisson–Boltzmann limit, the charge on a sphere may be approximated by the analytic expression, developed by Sader[43] (see eq25). For a constant surface potential, the predicted charge at small κR is linear in the radius, while at large κR the dependence becomes quadratic in R. Consequently, the charge polydispersity will approach asymptotically the size polydispersity at $\kappa R \ll 1$ and the limit $\langle\sigma_Z\rangle = 2\langle\sigma_R\rangle$ at large κR. The dashed region in Figure 3 brackets the predicted charge polydispersity assuming that the surface potential is fixed at the radius-independent value, determined in Figure 2, of $\Phi = 2.72$. The charge variation was calculated from the Sader expression (eq 25) using the experimentally measured radius polydispersity of $\langle\sigma_R\rangle = 0.046 \pm 0.01$. The agreement is reasonable given the uncertainities in the measured charge polydispersities and supports the picture of a constant surface potential, independent of both screening length and particle radius. To confirm the radius independence of Φ over a wider range of radii we prepared a number of differently sized particles and
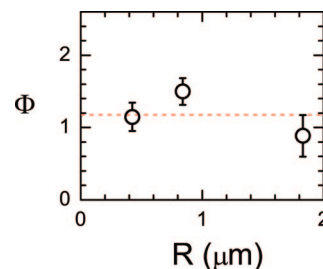

Figure 4. Variation of the dimensionless surface potential $\Phi = e\varphi/k_\mathrm{B}T$ with particle radius R. The PMMA particles were prepared using stabilizer B and the dispersions contained 100 mM of AOT. The surface potential was determined from electrokinetic measurements using the model of O'Brien and White. The data are consistent with a size-independent surface potential $\langle\Phi\rangle = 1.18 \pm 0.18$.

measured their mobilities in the presence of a fixed concentration of AOT (100 mM). Figure 4 shows the resulting variation in the surface potential Φ with particle radius. The data confirm the existence of a fixed particle potential, independent of size.

c. Adsorption of Surfactant. In recent years, the structures of amphiphiles at solid surfaces has been extensively studied using techniques such as neutron reflection, fluorescence spectroscopy, and atomic force microscopy. The molecular organization seen is surprisingly complex. A variety of structures have been proposed, ranging from spherical aggregates resembling bulk micelles, through cylinders and perforated layers, to uniform continuous layers.[44] While the self-assembly of surfactants on polar surfaces from aqueous solution has been extensively studied, a lot less attention has been paid to the adsorption of surfactants from organic solvents and the information, when available, is limited. For the specific case of the anionic surfactant, AOT, fluorescence studies[45] have revealed the presence of reverse "micelle-like" surfactant aggregates for adsorption onto hydrophobic graphite particles, from cyclohexane. The adsorption isotherm of the surfactant AOT on PMMA particles has been measured by Kitahara et al.[24] The adsorption increases sharply at low concentrations suggesting a high affinity of the surfactant for the surface of the particle before reaching a plateau value at high concentrations.

If surfactant micelles are adsorbed onto the surface of the particle then the number of free micelles in solution must decrease. Accordingly, we expect, from the charge fluctuation model, the number of charged micelles and thus the solution conductivity to decrease. To confirm this, we measured the conductivity of a dispersion of 42 nm particles with a constant colloid volume fraction, $\phi_c = 0.08$, suspended in a decane solution of AOT micelles. To increase the conductivity changes so they were easier to detect we increased the size of the reverse micelles by adding water, keeping the molar ratio w of water to AOT fixed at 40.8 so that the micelle radius was fixed. Small-angle neutron scattering measurements[34] indicate that, under these conditions, the reverse micelles have a radius of $r = 7.8$ nm which is independent of concentration. The conductivity σ and viscosity η of solutions of the swollen micelles in decane were measured as a function of the micelle volume fraction ϕ_m. The data displayed a linear dependence of $\sigma\eta$ upon ϕ_m, similar to the data on the dry micelles shown in Figure 1. The size of the swollen micelles is, however, considerably larger than the dry micelles so the proportion of micelles which are ionized is bigger. The fluctuating

(43) Sader, J. E. *J. Colloid Interface Sci.* **1997**, *188*, 508–510.

(44) Manne, S.; Gaub, H. E. *Science* **1995**, *270*, 1480–1482.
(45) Krishnakumar, S.; Somasundaran, P. *Colloids Surf.* **1996**, *117*, 227–233.
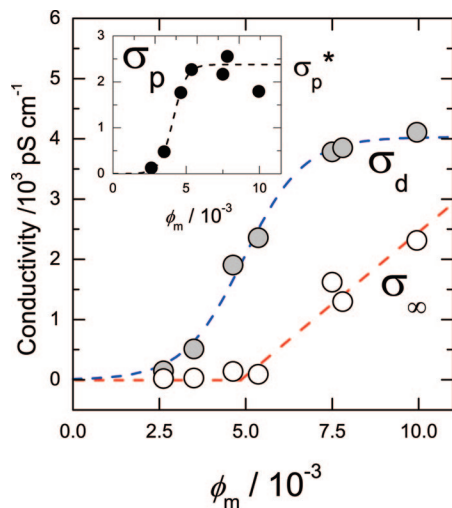
Figure 5. Conductivity of a suspension of small PMMA particles (RK1, $R = 42$ m) as a function of the volume fraction ϕ_m of swollen AOT reverse micelles in decane. The colloid volume fraction was fixed at $\phi_c = 0.08$. Filled circles: conductivity of suspension σ_d; open circles: conductivity of supernatant σ_∞; filled circles (inset): contribution to suspension conductivity from particles alone, $\sigma_p = \sigma_d - \sigma_\infty$. Note, for $\phi_m \leq 5 \times 10^{-3}$ the conductivity of the suspension is finite, although no micelles are detectable in the supernatant ($\sigma_\infty \approx 0$). This indicates that particles charge by the adsorption of charged micelles.

charge model has been modified by Hall[46] to take into account the discrete charging of multiply charged micelles. In this model, the predicted conductivity has the form of eq 9 but with

$$\chi = \frac{\Sigma_{z=-\infty}^{\infty} z^2 \exp(-\beta z^2 u_{el})}{\Sigma_{z=-\infty}^{\infty} \exp(-\beta z^2 u_{el})} \qquad (11)$$

where βu_{el} is the micelle charging energy and the micelle charge z takes discrete but arbitrarily large values. From a plot of $\sigma \eta$ against ϕ_m we determine $\chi = 0.22$ for the water-swollen micelles. Retaining in eq 11 the values $z = 0, \pm 1,$ and ± 2 the summation is readily inverted to give a micelle charging energy of $\beta u_{el} = 2.0$, in quite good agreement with the electrostatic prediction $\lambda_B/2r = 1.8$. The water-swollen AOT solution contains predominately uncharged and singly charged micelles. The proportion of doubly charged micelles is less than 0.06%.

The conductivity σ_d of a mixture of swollen micelles and particles has contributions from (1) the motion of the charged particles and their accompanying diffuse layer of micellar counterions (σ_p), and (2) the transport of excess micellar ions (σ_∞), so that $\sigma_d = \sigma_p + \sigma_\infty$. To distinguish these terms, we used centrifugation to separate the colloidal particles from excess micellar ions. The conductivity of the supernatant provides an estimate for σ_∞, since the neutral particle sediment must contain only the charged particles and the counterions required for charge neutrality, while σ_p was found by subtraction. Figure 5 shows the dependence of σ_p and σ_∞ on the volume fraction ϕ_m of reverse micelles added to the system. At low micelle concentrations ($\phi_m \leq 5 \times 10^{-3}$), no charged micelles remain free in solution, all are adsorbed, and the conductivity of the supernatant is essentially zero. The micelle-coated particles are clearly charged since σ_p, the contribution to the suspension conductivity from the particles alone, is nonzero and increases rapidly with increasing ϕ_m. As more micelles are added σ_p at first increases rapidly before finally saturating at $\sigma_p^* \approx (2.4 \pm 0.2) \times 10^3$ pS cm^{-1} at high micelle concentrations. The dependence of σ_p on the micellar volume

fraction, ϕ_m, is highly reminiscent of a Langmuir isotherm, with the rapid rise at low concentrations suggesting a high affinity interaction between particle and micelles. Comparing the dependence of σ_p and σ_∞ on the number of micelles added confirms that only when the particle surface is fully saturated with micelles ($\phi_m > 6 \times 10^{-3}$) does the number of free micelles in solution and thus the conductivity of the supernatant σ_∞ start to increase. The plateau in σ_p at high micelle concentrations (see inset in Figure 5) implies that the charge per particle is essentially constant for $\phi_m > 6 \times 10^{-3}$, or equivalently when about 12 micelles are adsorbed per particle. If the adsorbed micelles pack in a triangular tesselation on the surface then the maximum number of micelles that can be physically accommodated in a monolayer on each particle is $N = (2\pi/\sqrt{3})(R/r)^2$, or ~100 per particle for $r = 7.8$ nm and $R = 42$ nm. Accordingly, when the charge saturates the particle surface is only sparsely covered with micelles, with ~12% of the available surface sites occupied. The experimental system therefore is located in the $\theta < 1$ limit of the competitive adsorption model introduced in Section IV.a.

The plateau conductivity σ_p^* allows us to estimate the net charge carried by each micelle-coated particle. Using the experimentally determined micelle charge fraction χ, we estimate the Debye length at the conductivity plateau as $\kappa^{-1} \approx 70$ nm. Since the double layer is diffuse ($\kappa R = 0.6$), the charged particle and counterions move, to a first approximation, independently of each other in the applied field. The particle conductivity σ_p^* may therefore be expressed as

$$\sigma_p^* = \frac{Z_0^2 e^2}{6\pi\eta R} n_p + \frac{|Z_0| e^2}{6\pi\eta r} n_p$$

$$= \frac{e^2 \phi_c}{8\pi^2 \eta R^3 r}\left[\left(\frac{r}{R}\right) Z_0^2 + |Z_0|\right] \qquad (12)$$

where $n_p = 3\phi_c/4\pi R^3$ is the particle number density. Here the first term on the right-hand side of eq 12 arises from the motion of the particles, and the second term is due to counterions. Using this expression and the measured value of σ_p^* we estimate the mean charge of each particle as $4.1e$. While the particles used for the conductivity experiments are too small for measurements of the electrophoretic mobility, the equivalent dimensionless charge $Z_0\lambda_B/R$ is 2.8, in pretty good agreement with the value found for the larger 610 nm polymer particles by SPOM ($Z_0\lambda_B/R = 2.58 \pm 0.04$). This similarity between the particle charges found in the dry AOT and water-swollen AOT systems indicate that the presence of water does not significantly change the micelle adsorption energies.

IV. Charging Mechanism

In this section we analyze a charge regulation model of the micelle-decorated colloid, illustrated in Figure 6. We assume that oppositely charged micelles compete with each other and with uncharged micelles for the same binding sites on the surface of the particle. Using equilibrium statistical mechanics we examine the partitioning of positive and negatively charged micelles between solution and the particle surface and show that the model is consistent with the data presented in Section III. The model is essentially a variant of the classical charge regulation model of amphoteric surfaces first introduced by Chan et al.[47] and applied recently to particle charging by Strubbe and co-

(46) Hall, D. G. *J. Phys. Chem.* **1990**, *94*, 429–430.

(47) Chan, D.; Perram, J. W.; White, L. R.; Healy, T. W. *J. Chem. Soc., Faraday Trans. 1* **1975**, *71*, 1046–1057.
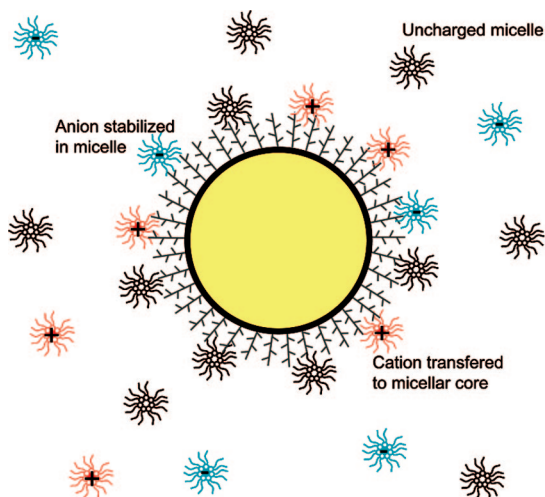
Figure 6. Micelle-decorated polymer particle. The decorated particle acquires a surface charge by the adsorption of an excess of either positively or negatively charged micelles.

workers.[48] Below we present a simple physical derivation of the charge regulation model which is tailored to the specific problem under consideration. For a more detailed general treatment, the reader is referred to the original paper.[47]

a. Competitive Adsorption of Charged Micelles. A nonpolar surfactant solution contains a random mixture of neutral and charged micelles. Reverse micelles frequently display a short-range attraction in organic media due to a mutual interpenetration of surfactant tails[49] or a solvent-mediated depletion interaction.[50,51] Similar attractive interactions probably operate between micelles and the hydrophobic polymer chains which coat a sterically stabilized colloid. As a result, we expect the surface of a particle to be decorated with a random mixture of charged and uncharged micelles. In our model the number of micelles that can adsorb is limited by N, the number of available surface sites per particle. The extent of absorption is controlled by M, the number of free micelles per particle. The net charge on the particle will fluctuate in time as the number of positively charged and negatively charged micelles adsorbed change as a result of exchange and/or charging reactions. We assume that the partitioning of micelles between surface and solution is determined purely by equilibrium energetics—the differences in free energy between adsorbed and free micelles of either positive Δg_P, negative Δg_N, or neutral charge Δg_U. Without loss of generality we consider the situation where $\Delta g_P < \Delta g_N$ so that positive micelles are more strongly adsorbed than negative micelles and the particle develops a net positive surface potential, φ. The particle charge becomes progressively more positive as more positive micelles adsorb. However, an electrostatic feedback limits the maximum charge. As micelles adsorb, the electrostatic repulsions between the particle and free positively charged micelles become increasingly dominant. At some point, approaching positive micelles are repulsed and micelles with the opposite sign are attracted to the particle surface. The charge on the particle is accordingly regulated by the competition of the different micellar species with each other for the available surface sites.

To analyze this situation, we focus on the energetics of adsorption of a single positive micelle onto a colloidal particle.

(48) Strubbe, F.; Beunis, F.; Marescaux, M.; Neyts, K. *Phys. Rev. E* **2007**, *75*, 031405.
(49) Lemaire, B.; Bothorel, P.; Roux, D. *J. Phys. Chem.* **1983**, *87*, 1023–1028.
(50) Pincus, P. A.; Safran, S. A. *J. Chem. Phys.* **1987**, *86*, 1644–1645.
(51) Cassin, G.; Badiali, J. P.; Pileni, M. P. *J. Phys. Chem.* **1995**, *99*, 12941–12946.

The chemical potential difference $\Delta\mu$ between adsorbed and free micelles has three contributions. First, there is the loss of the translational free energy when a micelle is bound to the particle surface. Offsetting this energetic cost is the gain in surface free energy as the micelle is adsorbed to any one of a large number of vacant surface sites. Finally, there are the energetic terms: the energy of adsorption, Δg_P, and the electrostatic energy $e\varphi$ arising from the Coulomb repulsion between the charged micelle and a particle with potential φ.

The translational entropy of the positively charged micelles after Z_P micelles have been absorbed on the surface of a particle is

$$-S_T = k_B\left[\left(\frac{M\chi}{2} - Z_P\right)\ln\left(\frac{M\chi}{2} - Z_P\right) - \left(\frac{M\chi}{2} - Z_P\right)\right] \quad (13)$$

where $M\chi/2 - Z_P$ is the remaining number of positive micelles in solution. The change in translational free energy per unit positive micelle is accordingly

$$-\beta T dS_T/dZ_P = -\ln(M\chi/2 - Z_P) \quad (14)$$

To estimate the configurational entropy of the surface phase of positive micelles we suppose there are Z_P ions and $N - Z_N - Z_U$ unoccupied sites. The total number of arrangements of the surface phase is

$$\Omega = \binom{N - Z_N - Z_U}{Z_P} = \frac{(N - Z_N - Z_U)!}{(N - \Sigma)!\, Z_P!} \quad (15)$$

where Σ is the total number of micelles adsorbed, $\Sigma = Z_P + Z_N + Z_0$. If we assume that all of these arrangements are equally probable, then the configurational entropy will include a term $S_C = k_B \ln \Omega$, which using Stirling's approximation reduces to

$$-k_B[Z_P \ln Z_P/(N - Z_N - Z_U) + (N - \Sigma)$$
$$\ln(N - \Sigma)/(N - Z_N - Z_U)] \quad (16)$$

Differentiation with respect to Z_P gives the surface entropy contribution to the free energy change per unit micelle as

$$-\beta T dS_C/dZ_P = -\ln(N - \Sigma)/Z_P \quad (17)$$

The equilibrium concentration of positive micelles is determined by the condition that the chemical potential of the charged micelles is the same at the surface as in solution. Combining the entropic (eqs 14 and 17) and energetic contributions gives the difference in chemical potential between bound and free positive micelles as

$$\beta\Delta\mu = -\ln(N - \Sigma)/Z_P - \ln(M\chi/2 - Z_P) + \beta\Delta g_P + \Phi \quad (18)$$

where $\Phi = e\varphi/k_B T$ is the dimensionless particle potential. In equilibrium $\Delta\mu = 0$. To simplify the equations from here on, we assume that the colloid concentration is sufficiently small that the number of free micelles exceeds the number adsorbed so that $\chi M/2 \gg Z_P$. This is a reasonable assumption in the case of the single-particle data presented in Section III. In this regime, eq 18 rearranges to an expression for the number of positive micelles adsorbed,

$$Z_P = M(N - \Sigma)K_P \exp(-\Phi) \quad (19)$$

where the equilibrium constant $K_P = \exp[-\beta(\Delta g_P + u_{el})]$ is independent of N and M. Note that K_P refers to the two-stage process; adsorption of an uncharged micelle onto the particle surface followed by ionization of the adsorbed micelle. Typically, $\Delta g_P + u_{el} > 0$ so the free energy of the adsorbed charge micelle is higher than the free micelle. As expected, eq 19 reveals that Z_P is a sensitive function of the surface potential, decreasing as

Φ becomes more positive due to the increased electrostatic repulsion between the positive micelle and positive surface.

Applying similar arguments to the adsorption of the negative and uncharged micelles yields expressions for Z_N and Z_U

$$Z_N = M(N - \Sigma)K_N \exp(\Phi)$$
$$Z_U = M(N - \Sigma)K_U \qquad (20)$$

with the corresponding equilibria constants

$$K_N = \exp[-\beta(\Delta g_N + u_{el})]$$
$$K_U = \exp[-\beta \Delta g_U]. \qquad (21)$$

Substituting eqs 19 and 20 into the definition of Σ and rearranging produces an explicit expression for Σ in terms of the unknown surface potential Φ,

$$\Sigma = \frac{MN[K_P \exp(-\Phi) + K_N \exp(\Phi) + K_U]}{1 + M(K_P \exp(-\Phi) + K_N \exp(\Phi) + K_U)} \qquad (22)$$

The number of charged micelles adsorbed depends upon the potential and is therefore unknown. Rather than specify the potential, we determine Φ self-consistently as follows. The equilibrium particle charge Z_0 is determined by the difference in the number of positive and negative micelles adsorbed upon the surface

$$Z_0 = Z_p - Z_N \qquad (23)$$

while the corresponding surface potential Φ is obtained from the solution of the nonlinear Poisson–Boltzmann (NLPB) equation,

$$\nabla^2 \Phi = \kappa^2 \sinh \Phi \qquad (24)$$

To circumvent the need for a full numerical solution of the NLPB equation, we use a simple yet accurate expression for the surface charge of a uniformly charged sphere introduced by Sader,[43]

$$\frac{Z_0 \lambda_B}{R} = \Phi(1 + \kappa R) - \frac{\tau_1^2 (\kappa R)^2}{\tau_2 - \tau_1 \kappa R} \qquad (25)$$

where $\tau_1 = 2 \sinh(\Phi/2) - \Phi$, $\tau_2 = 4 \tanh(\Phi/4) - \Phi$. In comparison with an exact numerical solution of the NLPB equation, the relative error in the surface charge predicted from 25 was found to be less than 1% over the entire range of κR for $\Phi \leq 6$.[43]

Substitution of eqs 19–23 into eq 25 yields an explicit expression for the particle potential Φ as a function of the number of free micelles in solution. The resulting nonlinear equation is readily solved numerically.[52] We limit our investigations to surface potentials of less than 150 mV (corresponding to scaled potentials $\Phi \leq 6$) since higher values are rarely encountered in nonpolar systems. The solutions reveal two limiting charging mechanisms depending upon whether the fractional coverage $\theta = \Sigma/N$ of the particle surface by micelles is small ($\theta \ll 1$) or if the surface is nearly saturated with adsorbed micelles ($\theta \lesssim 1$). Below, we discuss each situation in turn.

Low Surface Coverage ($\theta \ll 1$). In many practical instances, the number of sites for adsorption is significantly larger than the total number of micelles adsorbed ($N \gg \Sigma$) so that the particle surface is only sparsely covered with micelles. Typical numerical solutions for the surface potential Φ as a function of the number of micelles per particle M are depicted in Figure 7. The free energies of micelle adsorption are chosen so that particles charge
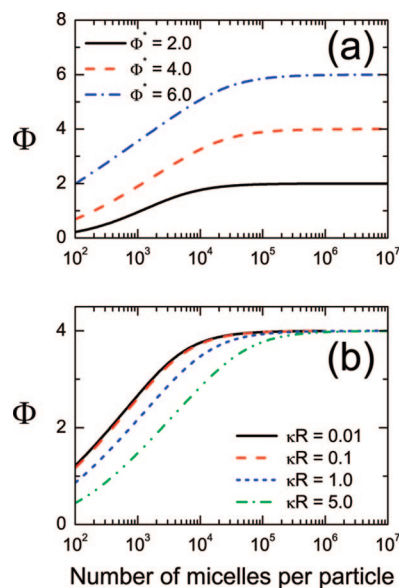
(52) Press, W.; Teukolsky, S. A.; Vetterling, W. T.; Flannery, B. P. *Numerical Recipes in FORTRAN, 2nd ed.*; Cambridge University Press: Cambridge, UK, 1992.


Figure 7. Saturation of the surface potential Φ by micelle adsorption. The curves correspond to typical solutions of eqs 19–23 and 25. Part (a) shows the calculated potential Φ for cases of *weak* adsorption (ln $K_P = -16$, ln $K_N = -20$; bottom solid curve), *moderate* adsorption (ln $K_P = -14$, ln $K_N = -22$; middle dashed curve), and *strong* adsorption (ln $K_P = -12$, ln $K_N = -24$; top dash-dotted curve). Other parameters: ln $K_U = -25$, $N = 10^6$, $R = 20\lambda_B$, and $\kappa R = 1$. Part (b) illustrates the dependence of the charging behavior on the inverse screening length κR. The curves depict the numerical NLPB solutions for ln $K_P = -14$, ln $K_N = -22$, ln $K_U = -25$, $N = 10^6$, and $R = 20\lambda_B$.

positive and the particle surface is unsaturated, i.e., $\theta \ll 1$ at all micelle concentrations considered. The values of Φ are plotted for *weak* (ln $K_P = -16$, ln $K_N = -20$; bottom solid curve), *moderate* (ln $K_P = -14$, ln $K_N = -22$; middle curve), and *strong* (ln $K_P = -12$, ln $K_N = -24$; top curve) adsorption of positively charged micelles. A fixed value of $R = 20\lambda_B$ was chosen for the particle radius and $\kappa R = 1$. Clearly, each of the three systems calculated display a very similar charging behavior. The equilibrium potential first increases monotonically with increasing M before Φ saturates at a plateau value $\Phi = \Phi^*$, which is unchanged by further addition of micelles. In the case of weak, moderate, and strong adsorptions, the plateau potential saturates at $\Phi^* = +2$, $+4$, and $+6$, respectively.

The physical processes which result in a constant surface potential $\Phi = \Phi^*$ at high micelle concentrations are illustrated in Figure 8. The equilibrium particle charge Z_0 and the number of adsorbed positive (Z_P) and negative micelles (Z_N) were calculated from eqs 19 and 20 and the numerically determined potential. The calculations assume moderate adsorption (ln $K_P = -14$, ln $K_N = -22$). Figure 8a reveals that the number of charged micelles adsorbed increases uniformly with micelle concentration and is essentially linear with M at high concentrations. However, the equilibrium particle charge Z_0, which is defined by the *difference* between the number of positive and negative micelles adsorbed, shows a very different dependence on M. Figure 8b shows that while the net charge Z_0 is initially proportional to M for low micelle concentration, it rapidly saturates at high micelle concentrations as a consequence of the electrostatic feedback mechanism. In this plateau regime, any further increase in M leads to more adsorption but crucially to an *equal* number of positive and negative micelles being adsorbed. Accordingly, $Z_P - Z_N$ does not vary with M and the net particle charge remains fixed. Essentially, the surface acts to buffer any increase in the number of free micelles in solution by adsorbing simultaneously both charged species. Clearly, this mechanism can only operate
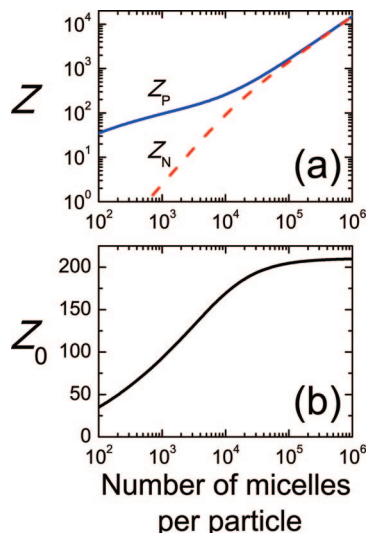
Figure 8. Competitive adsorption of charged micelles. Variation of (a) the number of adsorbed positive (Z_P) and negative (Z_N) micelles and, (b) the equilibrium particle charge (Z_0) with the number of free micelles per particle. The curves depict the numerical solutions of eqs 19, 20, and 25 for moderate adsorption. Parameters $R = 20\lambda_B$, $N = 10^6$, $\kappa R = 1$, $\ln K_P = -14$, $\ln K_N = -22$, and $\ln K_U = -25$ were used.

in the low coverage limit where empty sites remain on the particle.

Although the numerical calculations reported in Figures 7 and 8 use the NLPB equation to relate the surface potential to the adsorbed charge, the Debye−Hückel limit proves to be an extremely useful guide for understanding and approximating the charging mechanism. In the limit where the electrostatic potential is small compared with the thermal energy, $\Phi \ll 1$, the Poisson−Boltzmann equation (eq 24) may be linearized to give

$$\nabla^2 \Phi = \kappa^2 \Phi \qquad (26)$$

As is well known, the linearized Poisson−Boltzmann equation has an analytic solution.[53] In the limit where $\Phi \ll 1$, the particle charge is a linear function of the surface potential,

$$\frac{Z_0 \lambda_B}{R} = \Phi(1 + \kappa R) \qquad (27)$$

Using this expression rather than the more exact formula of eq 25 considerably simplifies the calculation of the equilibrium surface potential Φ so much so that the problem may be solved analytically. In the Debye−Hückel limit, $\Phi \ll 1$, the equilibrium surface potential Φ is the solution of the equation

$$\Phi = \frac{\lambda_B}{R(1 + \kappa R)} M(N - \Sigma)[K_P \exp(-\Phi) - K_N \exp(\Phi)] \qquad (28)$$

In the low coverage limit where $N \gg \Sigma$, eq 28 may be rewritten in the simple form,

$$\Phi = \alpha \sinh(\Phi^* - \Phi) \qquad (29)$$

where we have introduced the plateau potential Φ^*,

$$\Phi^* = \frac{1}{2}(\ln K_P - \ln K_N) = \frac{\beta}{2}(\Delta g_N - \Delta g_P) \qquad (30)$$

and the charging coefficient α,

(53) Verwey, E.; Overbeek, J. T. G. *Theory of the stability of lyophobic colloids*; Dover: New York, 1999.

$$\alpha = \frac{2\lambda_B}{R(1 + \kappa R)} MN\sqrt{K_P K_N}$$

$$= \frac{2\lambda_B}{R(1 + \kappa R)}\sqrt{Z_P Z_N} \qquad (31)$$

The resulting solution, the equilibrium potential Φ in the Debye−Hückel limit, has a simple graphical construction illustrated by the inset diagram of Figure 9. The equilibrium potential Φ is fixed by the intersection between the straight line $y = \Phi/\alpha$ and the curve $y = \sinh(\Phi^* - \Phi)$. A moment's reflection shows that, as the charging coefficient α increases, the equilibrium surface potential Φ approaches asymptotically the plateau potential Φ^*.

The saturation of the surface potential with increasing α in the Debye−Hückel limit is confirmed by the solution of eq 29—depicted for $\Phi = 1$ by the solid curve in Figure 9. The equilibrium potential first increases monotonically with increasing α before finally leveling off at $\Phi = \Phi^*$. In the plateau regime where $\alpha \gtrsim 10^2$, the predictions of the adsorption model are particularly simple. Here the surface potential is a constant, independent of the radius of the particle R, the micelle concentration M, the number of surfaces sites N, or the Debye length κ^{-1}. Indeed eq 31 reveals that the limiting potential Φ^* is a function *only* of the relative adsorption strengths of the surface for charged micelles and is totally unaffected by the composition of the system. Figure 9 also reveals, rather surprisingly, that the same features are also displayed by the full numerical NLPB solutions. The dashed curves in Figure 9 depict the NLPB solutions calculated for weak ($\ln K_P = -16$, $\ln K_N = -20$), moderate ($\ln K_P = -14$, $\ln K_N = -22$), and strong ($\ln K_P = -12$, $\ln K_N = -24$) absorption where the plateau potentials are $\Phi^* = 2$, 4, and 6 respectively. Even while linearization of the Poisson−Boltzmann equation is generally a poor approximation at high surface potentials ($\Phi \ll 1$), the dependence of Φ on the micelle concentration M is qualitatively unchanged when the Debye−Hückel approximation is used in place of the accurate Sader expression. This insensitivity is because the competition between oppositely charged micelles ensure the net particle charge changes rapidly with Φ in the vicinity of Φ^*. The predicted equilibrium potential is hence only slightly affected if the approximate Debye−Hückel expressions are used in place of accurate NLPB results.
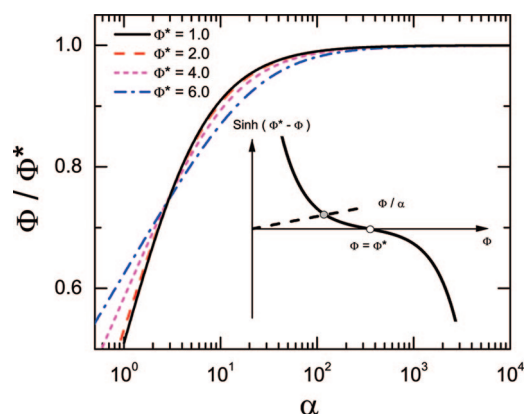

Figure 9. Equilibrium surface potential Φ, scaled by the plateau potential Φ^*, as a function of the charging coefficient α for competing micelle adsorption. The solid curve depicts the solution in the Debye−Hückel limit (eq 29) while the dashed curves correspond to the full NLPB solution (eqs 19–23 and 25). Note that in all cases Φ/Φ^* is almost independent of α when $\alpha \gtrsim 10^2$. The inset diagram gives a graphical depiction of the solution in the Debye−Hückel limit (eq 29).
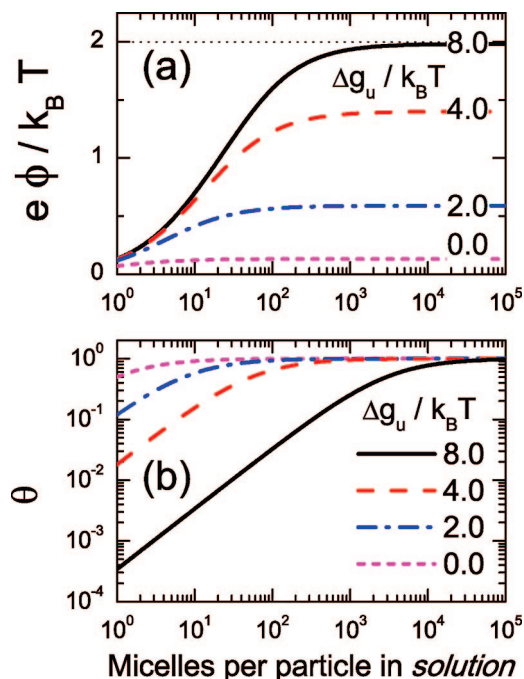
Figure 10. Dependence of (a) the equilibrium surface potential and (b) the fraction of surface sites occupied by micelles, upon the number of micelles per particle in solution. The curves are plotted for a number of different values for the uncharged micelle adsorption energy Δg_U. The dotted line in (a) is the saturated surface potential Φ^* according to eq 30. The results were computed from eqs 19–23 and 25 with $R = 20\lambda_B$, $N = 10^6$, $\ln K_P = -12$, $\ln K_N = -16$, and $\kappa R = 1$.

High Surface Coverage ($\theta \lesssim 1$). When the number of micelles adsorbed is comparable to the number of available surfaces sites then the calculation of the equilibrium potential Φ is more involved.

The effect on the surface potential of high degrees of micelle adsorption is illustrated in Figure 10. The plots were computed for a particle of radius $R = 20\lambda_B$ with $N = 10^6$, $\beta(\Delta g_P + u_{el}) = 12$, and $\beta(\Delta g_N + u_{el}) = 16$ in the regime $\kappa R = 1$. The fraction $\theta = \Sigma/N$ of the particle's surface covered by adsorbed micelles was varied by adjusting the adsorption energy Δg_U of uncharged micelles. If the uncharged micelles are only weakly adsorbed (for example, $\beta\Delta g_U = 8$) the surface is completely covered only at high micelle numbers, $M \geq 10^5$. In this case the surface potential Φ displays a similar dependence on M as that found previously (Figure 7) and Φ reaches the asymptotic limit, $\Phi = \Phi^*$. Increasing the number of uncharged micelles adsorbed by decreasing Δg_U has two consequences: (I) The surface potential saturates at a lower value ($\Phi < \Phi^*$) which decreases with increasing micelle adsorption, and (II) the concentration of micelles at which the potential saturates shifts to smaller M, as all absorption sites on the particle surface become occupied.

b. Analysis of Experimental Data. The analysis above demonstrates that the main physical quantity which controls the particle charge is the surface coverage θ. As shown by the conductivity data the experimental system of sterically stabilized PMMA particles in dodecane with added surfactant lies in the low surface coverage limit. The discussion of Section IV.a reveals that for low θ the surface potential is controlled by the charging coefficient α (eq 31). In the limit when $\alpha \lesssim 10^2$ the potential approaches the saturated value Φ^* and the charging mechanism becomes particularly simple. To identify if this is the case here, we estimate α. Under the conditions of the electrokinetic experiments ($\phi_m > 10^{-4}$, $\phi_c = 3 \times 10^{-5}$) the number of micelles per particle is $> 5 \times 10^8$. For AOT, the equilibrium constant K_N

for adsorption of negative micelles is of the order of $\exp(-\beta u_{el})$ and $K_P \approx \exp(-\beta u_{el} + 2\Phi)$, from eq 30, which implies that $\alpha \approx 10^7$. Consequently, we expect to be in the saturated potential limit where $\Phi = \Phi^*$. This is consistent with the experimental observations—namely that (a) the measured potential Φ does not depend on the concentration of reverse micelles (Figure 2); (b) the comparability of the charge and radius polydispersities seen in Figure 3; and (c) the surface potential is independent of R—trends predicted by the charge regulation model introduced in Section IV.a. Interpreting the measured surface potentials using eq 30 gives values for the free energy difference $\beta(\Delta g_N - \Delta g_P)$ for the adsorption of positive and negatively charged micelles of -5.4 ± 0.1 for AOT, $+6.4 \pm 0.4$ for Zr(Oct)$_2$ and 0.3 ± 0.3 for the PHSA–PMMA copolymer. The zero value, within error, for PHSA–PMMA is reasonable since in this case the micelles are chemically identical to the colloid-stabilizing layer and so we would expect no surface absorption. The preferential adsorption on PMMA of negative micelles, in the case of AOT, or positive micelles, in the Zr(Oct)$_2$ system, is more difficult to account for. We speculate that it may reflect different strengths of the charge-dipole interactions between the surfactant micelles and the dipole on the ester group of the poly(12-hydroxystearic) acid layer around each particle.[54] Work on different surfactant systems is necessary before the mechanism for preferential adsorption can be confirmed.

V. Conclusions

Micrometer-sized colloids may be charged in nonpolar solvents, despite their ultralow dielectric constant, by either the adsorption of ionic species or the dissociation of surface groups. The particle charge in a model system of sterically stabilized polymer colloids has been determined using SPOM. A key advantage of SPOM is that it yields accurate measurements of the extremely small mobilities of isolated *individual* colloidal particles typical of a nonpolar solvent such as dodecane. This technique yields information on the distribution of particle mobilities rather than simply recording the average mobility, as provided by most conventional electrokinetic techniques. The effect of particle size, the nature and concentration of the reverse micelles on the magnitude and sign of the colloid charge distribution has been investigated. We find surprisingly simple charging characteristics, in stark contrast with the rather complex behavior often reported for charging in nonpolar media (see for instance ref 24). In an extensive study, using three different reverse micellar systems and five differently sized particles, we find that the sign of the particle charge is determined by the chemical nature of the reverse micellar system. Interestingly, however, the magnitude of the surface potential was found to be unaffected by the concentration of micelles and to be independent of the colloid radius. These generic features suggest a common mechanism of charging operates in micelle containing dispersions.

To interpret our data, we suggest colloids charged by the competitive adsorption of oppositely charged reverse micelles. Within this model, the net charge Z_0 is determined by the *difference* in the number of positive and negative micelles absorbed onto the particle surface. The composition of the surface layer depends nonlinearly on the number of micelles in solution because oppositely charged micelles are preferentially attracted to the charged colloid. We analyze a simple equilibrium model of this competitive adsorption process and show that, with increasing micelle concentration, the surface potential rapidly saturates at a value $\Phi = \Phi^*$. The saturated surface potential Φ^*, is the

(54) Ottewill, R. H.; Rennie, A. R.; Schofield, A. *Prog. Colloid Polym. Sci.* **1990**, *81*, 1–5.

difference in the free energies of adsorption for negative and positive micelles in units of k_BT, $\Phi^* = \beta(\Delta g_N - \Delta g_P)/2$. Analysis of our experimental data using this model gives free energy differences of order $5-6$ k_BT, which look reasonable. Finally, we note that the model provides a coherent framework to understand and manipulate the charging of colloids in apolar solvents which will be highly beneficial for the future design of novel materials.

LA703908N